Accepted Manuscript

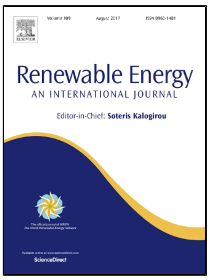

Numerical analysis of candidate materials for multi-stage metal hydride hydrogen compression processes

Evangelos I. Gkanas, Martin Khzouz

PII:	S0960-1481(17)30344-0
DOI:	10.1016/j.renene.2017.04.037
Reference:	RENE 8732
To appear in:	*Renewable Energy*
Received Date:	19 January 2017
Revised Date:	06 April 2017
Accepted Date:	19 April 2017

Please cite this article as: Evangelos I. Gkanas, Martin Khzouz, Numerical analysis of candidate materials for multi-stage metal hydride hydrogen compression processes, *Renewable Energy* (2017), doi: 10.1016/j.renene.2017.04.037

Highlights

- Numerical Study of multistage compressors
- Validation with solid experimental results
- Four different cases for two-stage compressor
- Comparison between two-stage and three-stage compressor

Numerical analysis of candidate materials for multi-stage metal hydride hydrogen compression processes

Evangelos I. Gkanas* and Martin Khzouz

Hydrogen and Mobility Lab, Centre for Mobility and Transport, Coventry University, Priory Street, Coventry CV1 5FB, United Kingdom.

* email: evangelos.gkanas.ac.uk

Abstract

A numerical study on multistage metal hydride hydrogen compression (MHHC) systems is presented and analyzed. Multistage MHHC systems use a combination of different materials to increase the final compression ratio at the end of the compression process. In the current work a numerical model is proposed to describe the operation of a complete three-stage MHHC cycle, which can be divided in seven steps (for a three-stage compression system): first stage hydrogenation process, sensible heating of first stage, coupling process between the first and the second stage, sensible heating of the second stage, second coupling with the upcoming sensible heating of the third stage material and finally the delivery of high pressure hydrogen to a high pressure hydrogen tank. Three scenarios concerning the combination of different materials for the compression stages are introduced and analyzed in terms of maximum compression ratio, cycle time and energy consumption. According to the results, the combination of $LaNi_5$ (stage 1), $MmNi_{4.6}Al_{0.4}$ (stage 2) and a novel synthesized AB_2-Laves phase intermetallic (stage 3) present a compression ratio 22:1 while operating between 20-130 ^oC.

Keywords: Metal Hydride Hydrogen Compressor; Heat and mass transfer; Hydrogenation/Dehydrogenation; Metal Hydrides;

1. Introduction

Energy is one of the key elements for global peace and nature rescue. An increase in the energy consumption of a country provides a positive impact on the economic as well as social development of the country [1, 2]. Over the past decade, the investigation for alternative fuels and energy technologies became important for the future energy stability [3, 4]. Hydrogen is one of the most promising energy carriers for the future energy needs. It is a high energy effective and low polluting fuel [5, 6]. Metal hydrides have been established as excellent mediums for hydrogen storage and compression applications compared to liquid and compressed hydrogen techniques due to the safest and more efficient operation [7].

The metal hydride technology for hydrogen compression has been an alternative to the use of conventional mechanical compressors. Current methods in hydrogen compression typically comprise of mechanical compressors operate in electricity derived from fossil fuels which poses higher energy costs. Compression of hydrogen gas to higher pressure, using mechanical compressors might face many technical problems related to lubrication, leakage, maintenance and compression construction. In addition, the mechanical compressors consume high grade of electrical energy for their operation.

With the implementation of metal hydrides for hydrogen compression, energy density and efficiency can be increased while reducing cost [8]. Compared to the conventional mechanical compressor, the hydrogen compressor based on reversible metal hydride presents many merits, such as the one of being able to export hydrogen over a wide range of pressure with high purity, free of mechanical movement or friction, low energy consumption, noiseless operation and easy and cheap maintenance [9-12]. The candidate materials for a metal hydride compressor need to present certain properties such as large reversible hydrogen storage capacity, flat plateau pressure, small hysteresis factor and high compression ratio [13-14]. Meanwhile, admirable reaction kinetics and pulverization resistance are also necessary [15]. The metal hydride hydrogen compressor is one such solution that can cover a wide range of operating pressures and pressure ratios by selecting suitable metal hydride combinations [16].

A multistage hydride-based compressor consists of a series of coupled modules containing metal alloys, which store and release the hydrogen gas in a cyclical manner,

under certain conditions of temperature and pressure. The driving force exerted by a variation in temperature which brings the transfer of hydrogen while increasing the exit pressure from the one stage to another. Despite the advantages of using metal hydride compression systems over the mechanical compressors, to become commercially available several things need to be achieved: the overall general efficiency of such systems needs to be improved and the capital cost to be significantly reduced [17]. Appropriate selection of the metal hydrides is essential to fully realize the commercial potential of the metal hydride compressor [18]. The multistage operation approach introduces more strict requirements to the tuneability of the Pressure-Composition-Temperature P-c-T characteristics, because during the coupling of the first stage (dehydrogenation) and the second stage (hydrogenation) the isotherms of both stages must be synchronized [19]. Some requirements for the correct selection is that the materials should present fast kinetics in order the compression cycle to be as fast as possible and relatively high reversible hydrogenation/dehydrogenation capacity, so the total amount for the materials needed to be lower. Low plateau slope for the isotherms of the materials, low hysteresis and cycle stability are also required. Finally, the cost of the compression process should be affordable.

Over the last decade, many scientists have made efforts in the subject of MHHC and some promising results were found both experimentally and numerically. Wang *et al*. [20] developed a 700-bar metal hydride compression system by using a two-stage system. For both stages, AB_2-type intermetallics based on Ti-Zr used. For the cooling/heating system cold/hot oil used and a compression ratio of 17.5:1 achieved operating between 25–150 ^{o}C. Li *et al.* [21] experimentally developed a two-stage metal hydride compressor by operating an AB_5-type intermetallic of the La-Ce-Ca-Ni family for the first stage and an AB_2-type of the Ti-Zr-Cr-Fe-V family and they concluded a final pressure of 745 bar at 150 ^{o}C with a compression capacity of 2000 L/cycle. Laurencelle *et al.* [22] reported a three-stage metal hydride compression system where for all the three stages AB_5-type intermetallics were selected based on the La-Ni-Sn, La-Ni and Mm-Ni-Al families respectively. Under operation temperatures between 20–80 ^{o}C a 20:1 compression ratio achieved. Popeneciu *et al*. [23] investigated a three-stage compressor and they reported that when the compressor operated between 20–80 ^{o}C the compression ratio was 28:1 when operating three AB_5-type intermetallics for the compression stages. Koultoukis *et al.* [24] studied experimentally potential AB_2-type

intermetallics based on the Ti-Zr family, applicable for hydrogen compression processes under several operating conditions. Furthermore, they also investigated [25] another series of AB_2-type intermetallics at operation range between 20–90 ^oC. Wang *et al*. [26] developed two alloys for hydrogen compression, an AB_5-type based on Ml-Mm-Ca-Ni and an AB_2-type based on Ti-Zr-Cr-Mn, where a compression ratio of 22.5:1 was reported. Several other works focusing on the numerical study of metal hydride compression were also reported. Muthukumar *et al*. [27] numerically studied the operation of a three-stage compression system using the AB_5-type $LaNi_5$, Mm-Ni-Al and an AB_2-type based on Ti-Zr-VFe-Cr-Mn as the operating metal hydrides between 20 and 120 ^oC and they reported a compression ratio of 28:1 at the end of the final stage. Gkanas *et al*. [28] investigated numerically the performance of a two-stage compression system by using an AB_5-type as the first stage material and an AB_2-type as the second stage material and they reported a compression ratio of 23:1 when operating the system between 20-130 ^oC. Furthermore, they investigated [29] numerically the performance of a three-stage compressor by using two AB_5-type intermetallics as the first and second stage materials and the commercial available Hydralloy C as the final stage material. Talaganis *et al*. [30] suggested a simplified model in order to reduce the number of the variables used during the simulation study. They used the proposed numerical model to simulate the compression behavior by using $LaNi_5$ and Mm-Ni-Al as the operating materials.

According to the previous studies there is a large interest in the experimental development of novel materials for effective hydrogen compression processes. The potential materials for such processes are based both on the AB_5-type intermetallics (such as $LaNi_5$, Mm-Ni-Al) as the materials for the first stages of the compression process and AB_2-type intermetallics as the materials to use for the upcoming stages and the final stage of the compression. On the other hand, there are not many publications focusing on the numerical analysis of the compression process and more specific on the usage of several materials to achieve the maximum compression ratio under the most suitable conditions of temperature and pressure for practical applications. In the current work, a numerical study of three-stage MHHC systems is presented and analysed. The proposed model was validated with experimental results extracted from a Sievert type apparatus. Three different MHHC systems were examined by using different combination of materials as the first, second and third stage in terms of maximum

compression ratio, cycle time and energy consumption for the operation of the system and the results extracted from the study are compared with previously reported results [28] regarding a two-stage compression system and discussing the necessity of the correct choice of materials and number of stages for the development of MHHC.

2. Model Formulation and Problem Definition

2.1 Introduction to a three-stage MHHC cycle

Figure 1 illustrates a simplified three-stage compression cycle and the van't Hoff diagram for all three stages, where the red lines correspond to the sensible heating process for each compression stage, the black dashed line to the hydrogenation process and the black lines to the dehydrogenation process for all stages respectively.

Fig.1. van't Hoff diagram describing the operation steps of a three-stage metal hydride hydrogen compressor and a simplified scheme of a three-stage compression system.

A full three-stage compression cycle can be summarized in seven simple steps:

Step 1: Valve 1 opens and the low pressure hydrogen supplier (electrolyser, hydrogen bottle..) is attached to first stage reactor. Hydrogen is stored to the first stage material in low pressure from the supplier until the hydrogenation process ends. Then valve 1 closes and the first stage reactor is in equilibrium.

Step 2: A sensible heating process of the first stage reactor occurs at a predefined high temperature (T_H) to increase the pressure inside the tank and prepare the system for the next step.

Step 3: Valve 2 opens between the first stage and the second stage. The temperature of the first stage reactor is high (T_H) and the temperature of the second stage is low (T_L) so a coupling process between the two-stages occurs. The released hydrogen from stage one at a relatively high pressure is stored in stage two. At the end of the coupling process valve 2 closes.

Step 4: Another sensible heating process takes place at a predefined high temperature (T_H) to increase the pressure inside the second stage reactor.

Step 5: Valve 3 opens between the first stage and the second stage. The temperature of the first stage reactor is high (T_H) and the temperature of the second stage is low (T_L) so a coupling process between the two-stages occurs.

Step 6: Sensible heating of the third reactor

Step 7: Valve 4 opens and high pressure hydrogen is stored in a high-pressure tank, while the first reactor is prepared (cooling) for the beginning of the upcoming compression cycle.

It is essential that the material selection should fulfil certain criteria to ensure that the operation of the compression system will be efficient and safe. As explained in Figure 2, the plateau pressure for the hydrogenation process of the first stage material should be sufficient low in order the material to be able to absorb the hydrogen from the low-pressure supplier. Furthermore, it is important that the plateau pressure of the dehydrogenation process for the first stage material should be higher than the plateau pressure for the hydrogenation process of the second stage material to ensure the presence of the pressure difference between the two reactors, which is going to act as the driving force to lead hydrogen from the first tank to the other. The same behavior must be presented during the second coupling process between the second and the third stage of the compression. Finally, to achieve the highest compression ratio, the plateau pressure of the final stage must be as high as possible.

Fig 2. P-c-T plot describing the operation steps of a three-stage metal hydride hydrogen compressor

2.2 Mathematical Model

To simplify the problem of hydrogen storage into the interstitial sites of the metal lattice which is a complex process containing chemical reactions, diffusion and heat transfer, it is essential to make some assumptions for the modeling purposes. The following assumptions have been considered for the current work.

a) Initially the temperature and pressure profiles are uniform inside the reactors.
b) Thermal conductivity and specific heat of the hydride are assumed to be constant during the compression cycle.
c) The medium is in local thermal equilibrium which implies that there is no heat transfer between solid and gas phases
d) Radiative heat transfer and viscous dissipation are negligible.
e) Hydrogen is treated as an ideal gas from a thermodynamic point of view.

2.3 Energy equation

Assuming thermal equilibrium between the hydride powder and hydrogen gas, a single energy equation is solved instead of separate equations for both solid and gas phases:

$$(\rho \cdot Cp)_e \cdot \frac{\partial T}{\partial t} + (\rho_g \cdot Cp_g) \cdot \overline{v}_g \cdot \nabla T = \nabla \cdot (k_e \cdot \nabla T) + m \cdot (\Delta H - T \cdot (Cp_g - Cp_s)) \quad (1)$$

Where m is the kinetic term. Normally, the last right-hand side term

$$m \cdot (\Delta H - T \cdot (Cp_g - Cp_s))$$

is referred as Heat Source term.

The effective heat capacity is given by:

$$(\rho \cdot Cp)_e = (\varepsilon \cdot \rho_g \cdot Cp_g) + ((1-\varepsilon) \cdot \rho_s \cdot Cp_s) \quad (2)$$

for the hydrogenation process and

$$(\rho \cdot C_p)_e = \rho_g \cdot Cp_g + \rho_s \cdot Cp_s \quad (3)$$

for the dehydrogenation process.

The effective thermal conductivity is updated by:

$$k_e = \varepsilon \cdot k_g + (1-\varepsilon) \cdot k_s \quad (4)$$

2.4 Hydrogen Mass Balance

The mass balance equation for hydrogen gas inside the reactor is described by the continuity equation as follows:

$$\varepsilon \cdot \frac{\partial(\rho_g)}{\partial t} + div(\rho_g \cdot \vec{v}_g) = -m \quad (5)$$

From the assumption that hydrogen is treated as an ideal gas, hydrogen density is considered from gases prefect law

$$\rho_g = \frac{P \cdot M_g}{R \cdot T} \quad (6)$$

2.5 Momentum equation

Gases velocity can be expressed by Darcy's law. By neglecting the gravitational effect, the equation which gives the velocity of gas inside the tank is given by:

$$\vec{v}_g = -\frac{K}{\mu_g} \cdot grad(\vec{P}_g) \quad (7)$$

Where K is the permeability of the solid and μ_g is the dynamic viscosity of gas. The solid permeability is given by the Kozeny–Carman's equation

$$K = \frac{dp^2 \cdot \varepsilon^3}{180 \cdot (1-\varepsilon^2)} \tag{8}$$

2.6 Kinetic expression

In the equations (1) and (5), the m term represents the amount of hydrogen that is stored and released in the materials.

For the hydrogenation process:

$$m_{abs} = C_{abs} \cdot \exp[-\frac{E_a}{R_g \cdot T}] \cdot \ln[\frac{p_g}{P_{eq}}] \cdot (\rho_{ss} - \rho_s) \tag{9}$$

Where C_a is the pro-exponential constant, E_a is the activation energy (calculated experimentally), ρ_{ss} is the saturation density of the hydride (after the full completion of the hydrogenation process) and ρ_s is the density of the hydride with time. The saturation density is determined by calculating the hydride concentration (mol/m^3) after the storage process and the volume of the hydride after the expansion process that occurs during the hydrogenation. As for the density of the hydride anytime, from the '*Transport of diluted species*' Module in COMSOL Multiphysics, the concentration of the hydride anytime is calculated (mol/m^3) and subsequently is substituted in Eq. (9) in order to calculate the kinetic term for the hydrogenation process.

For the dehydrogenation process:

$$m_{des} = C_{des} \cdot \exp[-\frac{E_d}{R_g \cdot T}] \cdot (\frac{P_{eq} - p_g}{P_{eq}}) \cdot \rho_s \tag{10}$$

Where C_d is the pro-exponential constant, E_d is the activation energy for the dehydrogenation process (measured experimentally) and ρs is the density of the hydride during the dehydrogenation process which is determined as for the hydrogenation process by calculating the concentration of the hydride and substituting in Eq. (10)

2.7 Equilibrium Pressure

Initially, the reactors are in equilibrium with the hydrogen gas. The hydride equilibrium pressure is estimated by using van't Hoff law [31]:

$$\ln P_{eq} = [\frac{\Delta \mathrm{H}}{R_g \cdot T} - \frac{\Delta S}{R_g} + (\sigma_s \pm \sigma_0) \cdot \tan(\pi(\frac{X}{X_{\max}} - \frac{1}{2})) \pm \frac{\mathrm{Y}}{2}] \cdot P_0 \tag{11}$$

Where σ_s and σ_0 are factors referring to the plateau slope flatness and Y is the hysteresis of the isotherm for the materials.

2.8 Coupled mass and energy balance

The situation of the system during the coupling between the first and the second stage after opening the valve between them is an important parameter that need to be considered when trying to describe the compression cycle. The number of moles inside the interconnector between the two reactors is updated from the following equation:

$$n_t = n_{in} + n_{des} - n_{abs} \tag{12}$$

To determine the number of moles, another '*Transport of diluted species*' Module in COMSOL Multiphysics to calculate the concentration of hydrogen (mol/m^3) during the hydrogenation process (Reactor 1), during the dehydrogenation process (Reactor 2) and at the interconnector between the two reactors.

The pressure of hydrogen inside the interconnector is updated by:

$$p_t = \frac{n_t \cdot R_g \cdot T}{V_1 + V_2} \tag{13}$$

Where V_1 and V_2 are the volumes of the first and second stage tanks respectively and T is the temperature of the gas inside the interconnector. Considering the pressure of hydrogen in the interconnector, we can use it as the driving force to lead hydrogen from the first stage to the second, therefore the kinetic equations for both hydrogenation and dehydrogenation process during the coupling are provided by the following equations.

$$m_{abs} = C_{abs} \cdot \exp(\frac{-E_a}{R_g \cdot T}) \cdot \ln(\frac{p_t}{P_{eq}}) \cdot (\rho_{ss} - \rho_s) \tag{14}$$

For the hydrogenation process.

$$m_{des} = C_{des} \cdot \exp(\frac{-E_d}{R_g \cdot T}) \cdot (\frac{P_{eq} - p_t}{P_{eq}}) \cdot (\rho_s) \tag{15}$$

For the dehydrogenation process.

3 Materials and Methods

3.1 Material Selection

Three different cases are studied regarding the proper material selection to build a three-stage MHHC. Table 1 presents all the studied cases. The first case utilizes $LaNi_5$ (AB_5-type) as the first stage alloy, $MmNi_{4.6}Al_{0.4}$ (AB_5-type) as the second stage alloy and Hydralloy C as the third stage. The second case uses $LaNi_5$ (AB_5-type) as the first stage alloy, $MmNi_{4.6}Al_{0.4}$ (AB_5-type) as the second stage alloy and a novel AB_2-intermetallic (Laves phase) as the third stage. The final case involves $MmNi_{4.6}Al_{0.4}$ (AB_5-type) as the first stage alloy, Hydralloy C as the second stage alloy and a novel AB_2-intermetallic (Laves phase) as the third stage. All the above mentioned

intermetallics were synthesized by arc-melting techniques and characterized by means of XRD (BRUKER AXS D8-Advance Diffractometer) and SEM (Zeiss NEON 40 EsB Microscope), in order to identify the microstructure of these materials and the P-c-T properties were measured by commercial Sievert-type apparatus (Hidden Isochema), in order to be able to measure the thermodynamic properties needed for the numerical calculations. For all the different cases the hydrogenation process was selected to occur at 20^{o}C and for the dehydrogenation process the temperature was selected at 130^{o}C. According to Table 1 and the analysis presented in chapter 2.1 for all the cases the temperature range is eligible for the compression applications.

Table 1. Cases used in the current study

3.2 Geometry of the system

The schematic of the metal hydride reactors used in the current computational study is shown in Figure 3. The geometry of each reactor is cylindrical and each reactor was chosen to be 50% full, to avoid any lattice expansion issues during the hydrogenation and dehydrogenation process. The target of this work is to achieve storage and compression of 60 g of hydrogen per compression cycle. In order to store 60g of hydrogen per compression cycle, the amount of the materials should be the following: 4.45 kg for $LaNi_5$, 4.12 kg for $MmNi_{4.6}Al_{0.4}$, 3.33 kg for Hydralloy C and 3.42 kg for the AB_2-intermetallic. For simplicity reasons, the porosity of all the materials was chosen 0.5 (the void volume inside the material to be 50%). At the center of the tank there is a hydrogen supply porous sintered filter which delivers hydrogen during the hydrogenation process and removes the released hydrogen during the dehydrogenation process. The length of each reactor was selected L=0.6m and the internal radius R=3.3cm. The cooling and heating of the tanks for the hydrogenation and dehydrogenation process was achieved by the usage of an external jacket, and the thickness of the tank walls was chosen to be 3mm which are identical to the dimensions of commercially available cylinders.

Fig3. The geometry of the reactors used in the current computational study. A cross-section of the reactor (left) shows that the hydride is inside the reactor and the thickness of the walls of the tank chosen to be 3mm. The heating and cooling process is achieved by an external jacket in the current case.

3.3 Validation of numerical results

For the validation of the proposed numerical model, a comparison between experimental and simulation data extracted from the numerical model was performed.

The experimental data collected using $LaNi_5$, $MmNi_{4.6}Al_{0.4}$, Hydralloy C and the AB_2 intermetallic as the operating materials at several temperatures by a commercial Sievert-type apparatus (Hidden Isochema). Figure 4 shows the temperature profile during the hydrogenation process (Figure 4a) and the hydrogenation profile (Figure 4b) when using the AB_2-Intermetallic as the operating material, where the lines (black color) represent the simulation results and the dots (color) represent the experimental data. It is observed that the numerically predicted temperature and hydrogenation behavior are in very good agreement with the experimental results.

Fig. 4. Validation of the numerical data extracted from the simulation to the experimental results for the synthesized AB_2-Intermetallic. Fig. 4a shows the temperature distribution and Fig. 4b the evolution of the hydrogenation process.

4 Results and Discussion.

4.1 *Temperature evolution of a complete three-stage compression cycle*

A complete three-stage hydrogen compression cycle consists of one independent hydrogenation process of the first stage hydride and a subsequent sensible heating, followed by a coupled dehydrogenation-hydrogenation process between the first and the second stage, the sensible heating of the second stage, a second coupling process between the second and third stage with the sensible heating of the third stage, and finally the dehydrogenation process of the third stage, where high pressure and purity hydrogen is released in the high pressure storage tank. The sensible heating process is necessary prior each dehydrogenation process to increase the equilibrium pressure to enhance and accelerate the dehydrogenation process. Figure 5 shows the bed average temperature evolution for the complete three-stage cycle with time when using $LaNi_5$ as the first stage, $MmNi_{4.6}Al_{0.4}$ as the second stage and the novel AB_2-intermetallic as the third and final stage (Case 2). The sensible heating process is described by the vertical black dashed line. During the initial stage of the hydrogenation process for the first stage hydride, due to the exothermic nature of the hydrogenation reaction that takes place, a sudden rise at the bed's temperature is observed, followed by a gradually decrease towards to the external jacket's temperature due to the thermal management of the reactor. This behavior can be explained due to the poor thermodynamic properties of the hydride powders and especially due to the poor thermal conductivity that the metal hydride powders present which does not allow the generated amount of heat to

be transferred from the hydride bed to the external jacket during the first stage of the hydrogenation process and the amount of heat is stored inside the metal hydride bed, resulting in a sudden rise of the temperature at the first stage of the hydrogenation. After the hydrogenation process, a sensible heating of the hydride bed takes place where the equilibrium pressure of the material increases. During the initial stage of the dehydrogenation process, the necessary amount of heat has not been transferred from the external heater (130^{o}C) to the hydride bed due to poor thermal conductivity and initially the necessary amount of heat is provided by the hydride bed itself, resulting in a sudden decrease of beds' temperature as illustrated in Figure 5. Therefore, a sensible heating process is essential for the dehydrogenation. Due to the increase of the heat within the hydride bed, according to the vant Hoff's law (Eq. 11), the sensible heating can increase the equilibrium pressure resulting in a favorable condition for the upcoming coupled dehydrogenation-hydrogenation process.

Fig. 5. Bed average temperature evolution during the complete three-stage compression process when using $LaNi_5$, $MmNi_{4.6}Al_{0.4}$ and AB_2-Intermetallic as the stages of the compression.

4.2 Pressure and storage capacity evolution during the complete three-stage compression cycle

The average pressure of the operating metal hydride beds during the three-stage compression cycle when using $LaNi_5$ as the first stage, $MmNi_{4.6}Al_{0.4}$ as the second stage and the novel AB_2-intermetallic as the third and final stage is presented in Figure 6. Initially, a low-pressure hydrogen supplier (e.x an electrolyser) is attached to the first stage hydride and provide hydrogen at pressure 15 bar and enters the first stage hydride due to the pressure difference. By maintaining the temperature of the first stage at low levels, hydrogen is stored at the lattice of the material indicating a gradually reduction of the hydrogen pressure within the storage bed during the first step of the pressure evolution. The pressure of hydrogen inside the first stage at the end of the hydrogenation process is almost 7 bar. After the hydrogenation, a sensible heating of the reactor occurs. During this process, there is a sharp increase in the bed's pressure, due to the increase of the equilibrium pressure as per vant Hoff's law. After the sensible heating process, the coupled dehydrogenation-hydrogenation procedure takes place. During the initial stage of this process, the equilibrium pressure of the dehydrogenating reactor decreases while the equilibrium pressure for the hydrogenating reactor increases sharply due to the very fast kinetics between the two reactors. After this rapid initial

stage of this coupled process, the pressure inside both the coupling reactors is increasing due to the presence of a driving potential. This process is described accurate at the inlaid picture of Figure 6. At the end of the first coupled process the pressure is 38-39 bar at the second reactor and a subsequent sensible heating process occurs where the pressure increases up to 110 bar. Then, the second coupling process between the second (dehydrogenation) and third (hydrogenation) stage begins, where the behavior is similar with the behavior described for the first coupling; the difference is that the second coupling takes place at a higher-pressure range. The pressure of hydrogen after the second coupling is almost 89 bar. Finally, during the final dehydrogenation process of the third stage to the high-pressure hydrogen tank the final hydrogen delivery pressure is almost 320 bar indicating a pressure ratio of 22:1 when the compressor operates between 20-130^{o}C.

Fig. 6. Bed average pressure evolution during the complete three-stage compression process when using $LaNi_5$, $MmNi_{4.6}Al_{0.4}$ and AB_2-Intermetallic as the stages of the compression.

Finally, Figure 7 presents the hydrogenation/dehydrogenation capacity for the complete compression cycle with time.

Fig. 7 Bed average hydrogenation/dehydrogenation evolution during the complete three-stage compression process when using $LaNi_5$, $MmNi_{4.6}Al_{0.4}$ and AB_2-Intermetallic as the stages of the compression.

4.3 Comparison of the different MHHC cases

The results that presented at chapters *4.1* and *4.2* referred to the MHHC system that utilizes $LaNi_5$ as the first stage hydride, $MmNi_{4.6}Al_{0.4}$ as the second stage and a novel AB_2-Intermetallic at the third stage. Furthermore, the operation temperatures for the compressor were 20^{o}C (hydrogenation) and 130^{o}C (dehydrogenation). Table 2 presents the outcome for the three different cases of MHHC systems that described at chapter 3.1, in terms of maximum compression ratio and cycle time. According to these results, it is obvious that all the studied cases present advantages and disadvantages for carrying out hydrogen compression operation. For the first case ($LaNi_5$, $MmNi_{4.6}Al_{0.4}$ and Hydralloy C) the maximum compression ratio achieved is 19:1 resulting on a final pressure 272 bar, where the duration for the completion of a full compression cycle is 220 min. For the second case ($LaNi_5$, $MmNi_{4.6}Al_{0.4}$ and AB_2-Intermetallic) the

maximum compression ratio achieved was 22:1 while the cycle time is quite faster than the first case (215 min). The energy consumption for the first two cases is almost similar as the time for the completion of the compression cycle is close. The results for the third case ($MmNi_{4.6}Al_{0.4}$, Hydralloy C and AB_2-Intermetallic) showed an even higher compression ratio 23:1 with a final delivery hydrogen pressure 320 bar, but on the other hand the duration for the compression cycle was 280 min, which was the slowest of all the studied cases and is expected to present the highest energy consumption as well.

Table 2. Comparison of the operation for the four different MHHC cases

4.4 Differences between three-stage and two-stage compression systems

Both a two-stage and a three-stage compression system operates under the same mechanism using metal hydrides to compress hydrogen. Their only difference is the number of the different stages during the operation. It is preferable to use a three-stage compression system when strict requirements in the temperature and pressure arise. For example, if on a compressor prototype the cooling/heating system is based on cold/hot water respectively, then is not possible to operate the system at the temperature ranges over 90-95^{o}C during the dehydrogenation process, thus the compression ratio when using a two-stage compressor will be relatively small according to a previous analysis [28]. The solution to the above engineering problem might be the addition of another material suitable for the applicable conditions. As already mentioned, the proper selection of the materials is crucial for the effective operation of the compressor in order to achieve the maximum driving force during the coupling between the stages. Thus, the operation of a three-stage system can provide a flexibility on the material usage comparing to a two-stage compressor. For example, by comparing the results of using a three-stage compressor (Case 2) between 20-130^{o}C to compress 60g of hydrogen where the compression ratio was found 22:1 to the results for a two-stage compression system [28], where an almost similar compression ratio was found, it is obvious that for the usage of a two or three-stage system someone needs to decide about the parameters need to be sacrificed in order to achieve the final target. For a three-stage system, the duration of the compression cycle is higher and the energy consumption is also higher as more modules need to be thermodynamically and mechanically treated. On the other hand, due to the fact that the pressure doesn't have to be increased directly, but involves an intermediate stage, a three-stage compressor offers more flexibility and

choices on the material selection, while for the two-stage compression the material selection has to be very strict and the choices might not be plenty. Thus, it is obvious that the selection of the proper compression system depends on a number of parameters such as the compression ratio, the cycle time, the operation conditions, the size and the energy consumption.

5 Conclusions

A numerical model describing the complete operation of a three-stage hydrogen compression system was presented and analyzed. The numerical results were validated with experimental data and very good agreement for both the temperature evolution and the hydrogenation profile was obtained. Three different cases of MHHC systems were studied and compared in terms of compression ratio, cycle time and energy consumption and was found that the operation temperature range for the compressor such as the choice of different materials as the operating hydrides can affect the compression characteristics. It was also found that when operating $LaNi_5$ as the first stage hydride, $MmNi_{4.6}Al_{0.4}$ as the second stage and a novel AB_2-intermetallic as the third stage alloy at a temperature range 20^{o}C (hydrogenation) and 130^{o}C (dehydrogenation) the final compression ratio could be almost 22:1 reaching at the end of the final dehydrogenation process a delivery pressure of 315 bar. In order to optimize the compression system and to able to achieve higher compression ratios while minimize the operation temperature ranges and consequently the energy consumption and to achieve faster cycle time special attention should be given to the research for materials with better compression characteristics (fast kinetics, low plateau slope and hysteresis, thermodynamics) and to the heat management of the metal hydride tank.

1

Nomenclature

C_a	*Absorption Reaction Constant, s^{-1}*
C_d	*Desorption Reaction Constant, s^{-1}*
C_p	*Specific Heat, J/kg-K*
E_a	*Activation Energy for Absorption, $J/molH_2$*
E_d	*Activation Energy for Desorption, $J/molH_2$*
h	*Heat Transfer Coefficient, W/m^2K*
k	*Thermal Conductivity, W/m-K*
K	*Permeability, m^2*
M	*Molecular Weight, kg/mol*
m	*Kinetic Expression*
n	*Number of Hydrogen Moles*
P	*Pressure, bar*
R	*Gas Global Constant, J/mol-K*
t	*Time (s)*
T	*Temperature (K)*
v	*Gas Velocity, m/s*
V	*Volume, m^3*

Subscripts

a	*Absorption*
A	*Reactor A*
B	*Reactor B*
d	*Desorption*
e	*Effective*
eq	*Equilibrium*
f	*External Heater/Cooler*
g	*Gas*
i	*Initial*
s	*Solid*
ss	*Saturation*

Greek Letters

ε	*Porosity*
μ	*Dynamic Viscosity, kg/ms*
ρ	*Density, kg/m^3*
ΔH	*Reaction Enthalpy, J/mol*
ΔS	*Reaction Entropy, J/mol-K*

17

18

19

20

21

22

23

24

25

26

References

[1] Dincer, I. (2007). Environmental and sustainability aspects of hydrogen and fuel cell systems. International Journal of Energy Research, 31, 29-55.

[2] Gkanas, E.I., Steriotis, T.A., Stubos, A.K., Myler, P. Makridis, S.S. (2015). A complete transport validated model on a zeolite membrane for carbon dioxide permeance and capture. Applied Thermal Engineering, 74, 36-46.

[3] Midili, A., Ay, M., Dincer, I. & Rosen, M.A. (2005). On hydrogen and hydrogen energy strategies II: Future projections affecting global stability and unrest. Renewable and Sustainable Energy Reviews, 9(3), 273-287.

[4] Midili, A. & Dincer, I. (2007). Key strategies of hydrogen energy systems for sustainability. International Journal of Hydrogen Energy, 32, 511-524.

[5] Gkanas, E.I, Makridis, S.S. (2016). Effective thermal management of a cylindrical MgH_2 tank including thermal coupling with an operating SOFC and the usage of extended surfaces during the dehydrogenation process. International Journal of Hydrogen Energy, 41, 5693-5708.

[6] Gkanas, E.I, Grant D.M., Khzouz, M., Stuart, A.D., Manickam K., Walker, G.S. (2016). Efficient hydrogen storage in up-scale metal hydride tanks as possible metal hydride compression agents equipped with aluminium extended surfaces. International Journal of Hydrogen Energy, 41, 10795-10810.

[7] Golben M. & Da Costa, D. (2002). Proceedings of the 2001 DOE hydrogen Program Review. http://www1.eere.energy.gov/hydrogenandfuelcells/annual_review2001.html

[8] Muthukumar, P., Linder, M., Mertz, R. & Laurien, E. (2009). Measurement of thermodynamic properties of some hydrogen absorbing alloys. International Journal of Hydrogen Energy, 34, 1873-1879.

[9] M.V. Lototskyy, V.A. Yartys, B.G. Pollet, R.C. Bowman Jr. (2014) Metal hydride hydrogen compressors: A review, International Journal of Hydrogen Energy, 39, 5818-5851.

[10] Makridis, S.S., Gkanas, E.I., Panagakos, G., Kikkinides, E.S., Stubos, A.K., Wagener, P., Barcikowski, S. (2013). Polymer-stable magnesium nanocomposites prepared by laser ablation for efficient hydrogen storage, International Journal of Hydrogen Energy, 38, 11530-11535.

[11] Yu, S., Ivanovsky F., Lotovsky, A.I., Karnatsevich, M.V., Milenko, L.V. & Yu, Y. (1999). Cryo – Hydride high pressure hydrogen compressor. International Journal of Hydrogen Energy, 24, 649-650.

[12] Bowman, R.C. Jr. (2003). Development of metal hydride beds for sorption cryocoolers in space applications. Journal of Alloys and Compounds, 356-357, 789-793.

[13] Shafiee, S., McCay, M.H. (2016) Different reactor and heat exchanger configurations for metal hydride hydrogen storage systems – A review. International Journal of Hydrogen Energy, 41, 9462-9470.

[14] Muthukumar, P., Patil, M.S., Raju, N.N., Imran, M. (2016) Parametric investigations on compressor-driven metal hydride based cooling system. Applied Thermal Engineering, 97, 87-99.

[15] Sharma, V.K., Kumar, E.A. (2016) Thermodynamic analysis of novel multi stage multi effect metal hydride based thermodynamic system for simultaneous cooling, heat pumping and heat transformation. International Journal of Hydrogen Energy (2016), http://dx.doi.org/10.1016/j.ijhydene.2016.09.154.

[16] Bowman Jr, R.C. (2003) Development of metal hydride beds for sorption cryocoolers in space applications. Journal of Alloys and Compounds 356-357, 789-793.

[17] Lototskyy, M.V, Klochko, Ye., Linkov, V., Lawrie P., Pollet, B.G. (2012) Thermally Driven Metal Hydride Hydrogen Compressor for Medium-Scale Applications. Energy Procedia 29, 347-356.

[18] Lototskyy, M.V (2016) New model of phase equilibria in metal – hydrogen systems: Features and software. International Journal of Hydrogen Energy 41, 2739-2761.

[19] Lototskyy, M.V, Yartys, V.A., Pollet, B.G., Bowman Jr, R.C. (2014) Metal hydride hydrogen compressors: A review. International Journal OF Hydrogen Energy 39, 5818-5851.

[20] Wang, X., Liu, H. & Li, H. (2011). A 70MPa hydrogen – compression system using metal hydrides. International Journal of Hydrogen Energy, 36, 9079-9085.

[21] Li, H., Wang, X., Dong, X., Xu, L. & Chen, C. (2010). A study on 70MPa metal hydride hydrogen compressor. Journal of Alloys and Compounds, 502, 503-507.

[22] Laurencelle, F., Dehouche, Z., Morin, F. & Goyette, J. (2009). Experimental study on a metal hydride based hydrogen compressor. Journal of Alloys and Compounds, 475, 810-816.

[23] Popeneciu, G., Almasan, V., Coldea, I., Lupu, D., Misan, I. & Ardelean, O. (2009). Investigation on a three – stage hydrogen thermal compressor based on metal hydrides. Journal of Physics, 182, 2009.

[24] Koultoukis, E.D., Gkanas, E.I., Makridis, S.S., Christodoulou, C.N., Fruchard, D., Stubos, A.K. (2014). High Temperature Activated AB_2 Nanopowders for metal Hydride Hydrogen Compression. International Journal of Energy Research 38, 477-486, 2014.

[25] Koultoukis, D. E., Makridis, S. S., Fruchart, D., Stubos, K. A. (2013). Two stage compression using Zr-based metal hydrides. Solid State Phenomena, 194, 249-253.

[26] Wang, X., Chen, R., Zhang, Y., Changpin, C. & Wang, Q. (2006). Hydrogen storage alloys for high pressure suprapure hydrogen compressor. Journal of Alloys and Compounds, 420, 322-325.

[27] Muthukumar, P., Patel, K.S., Pratik, S. & Singhal, N. (2012). Computational Study on metal hydride based three–stage hydrogen compressor. International Journal of Hydrogen Energy, 37, 3797 – 3806.

[28] Gkanas, E.I., Grant, D.M., Stuart, A.D., Eastwick C.N., Book, D., Walker, G.S. (2015) Numerical study on a two-stage Metal Hydride Hydrogen Compression system. Journal of Alloys and Compounds 645: S18 – S22.

[29] Gkanas, E.I., Makridis, S.S., Stubos, A.K. (2013). Modeling and Simulation for Absorption-Desorption Cyclic Process on a Three -Stage Metal Hydride Hydrogen Compressor. Computer Aided Chemical Engineering, 32, 379-384.

[30] Talaganis, B.A., Meyer, G.O., & Aguirre, P.A. (2011). Modeling and simulation of absorption–desorption cyclic processes for hydrogen storage–compression using metal hydrides. International Journal of Hydrogen Energy, 36, 13621-13631.

[31] Nishizaki, T., Miyamoto, K., Yoshida, K. (1983). Coefficients of performance of hydride heat pumps. Journal of Less Common Metals, 89, 559-566.

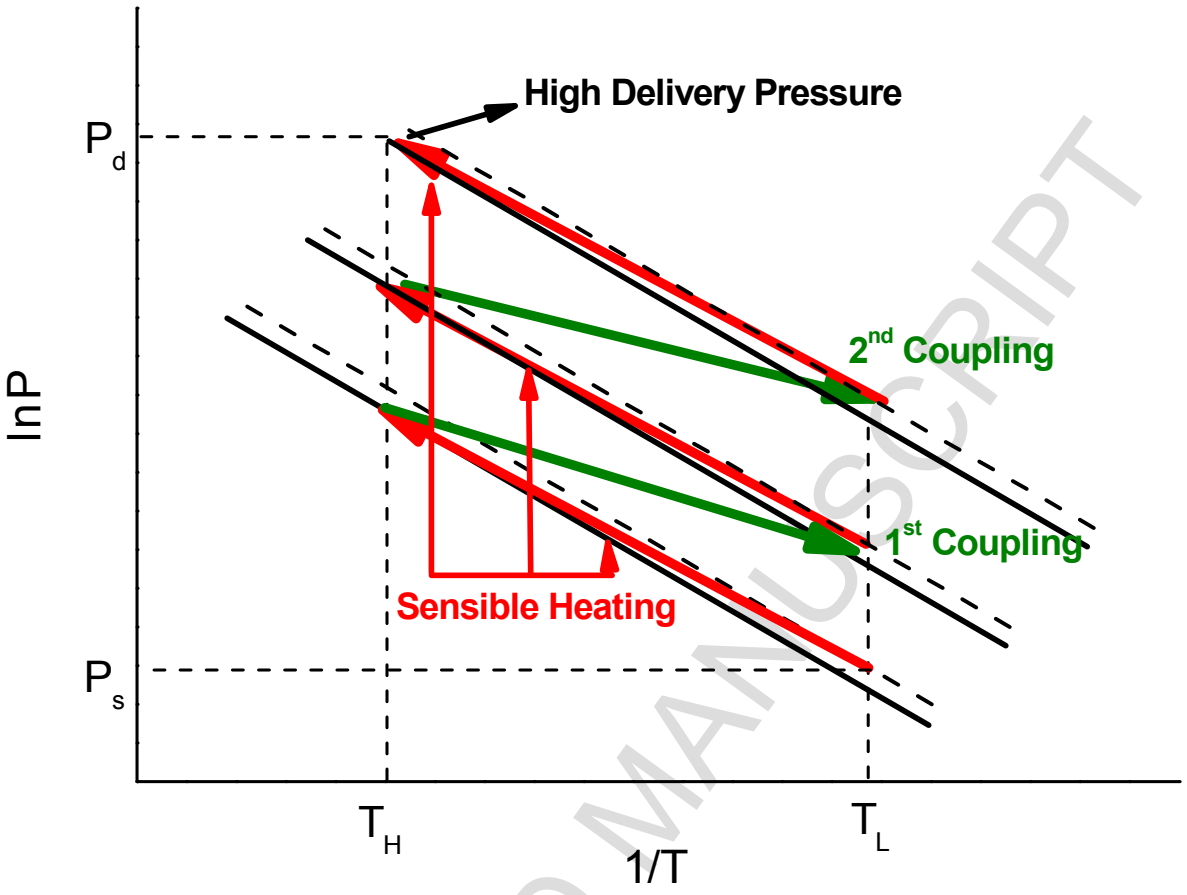

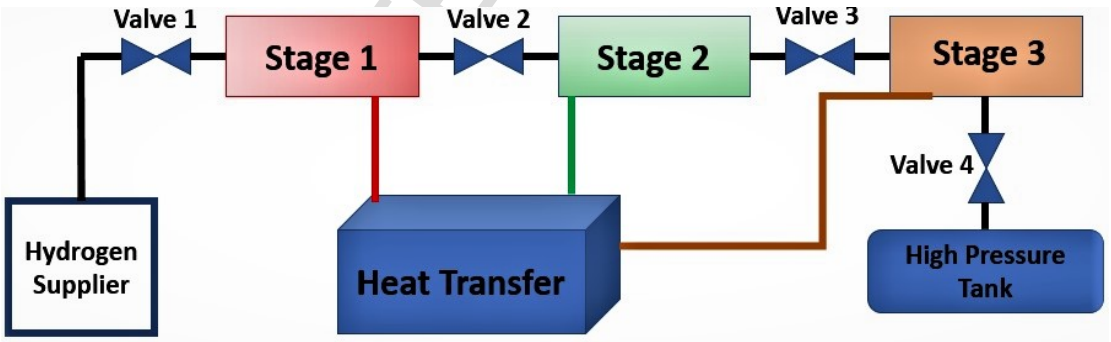

Fig.1. van't Hoff diagram describing the operation steps of a three-stage metal hydride hydrogen compressor and a simplified scheme of a three-stage compression system.

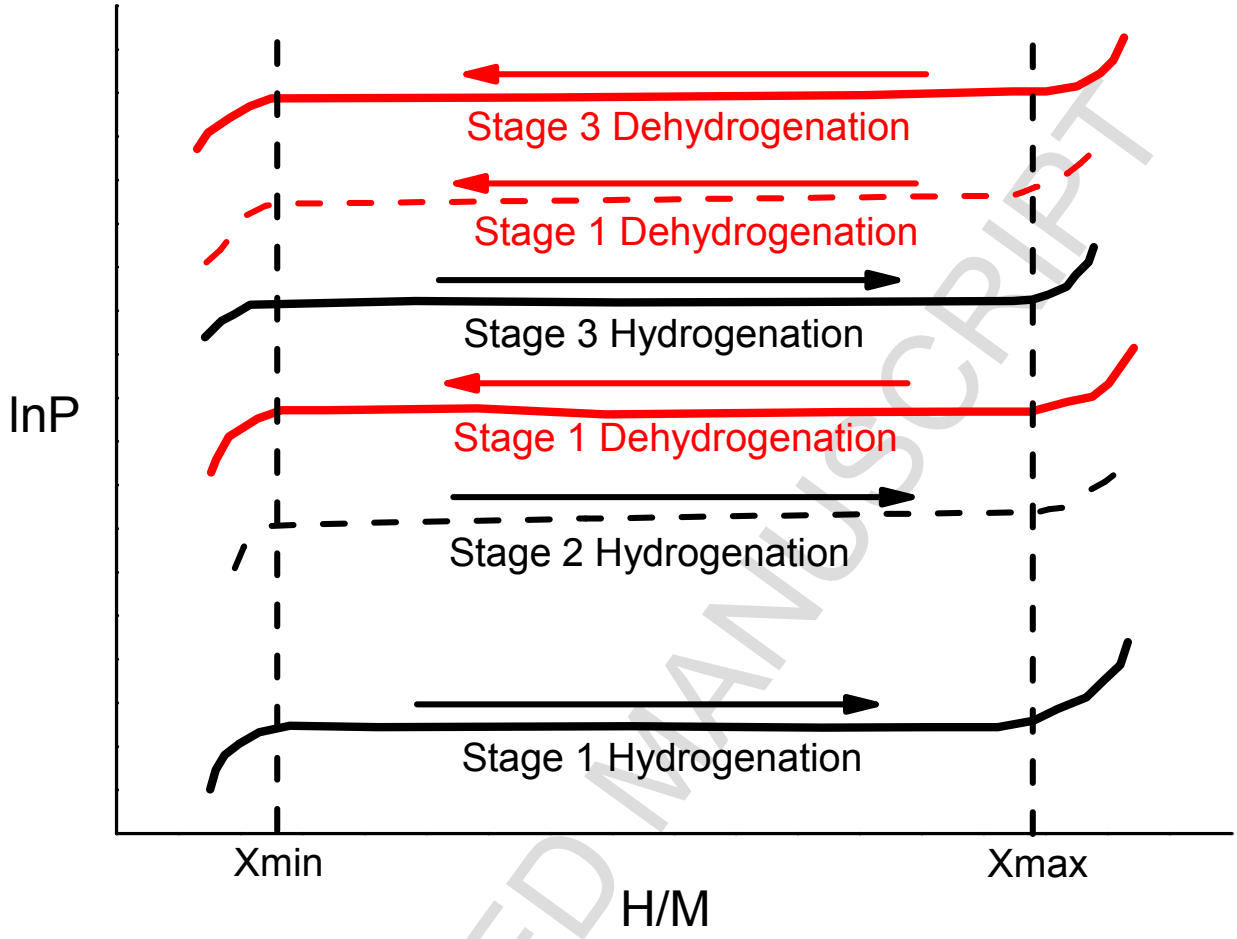

Fig 2. P-c-T plot describing the operation steps of a three-stage metal hydride hydrogen compressor

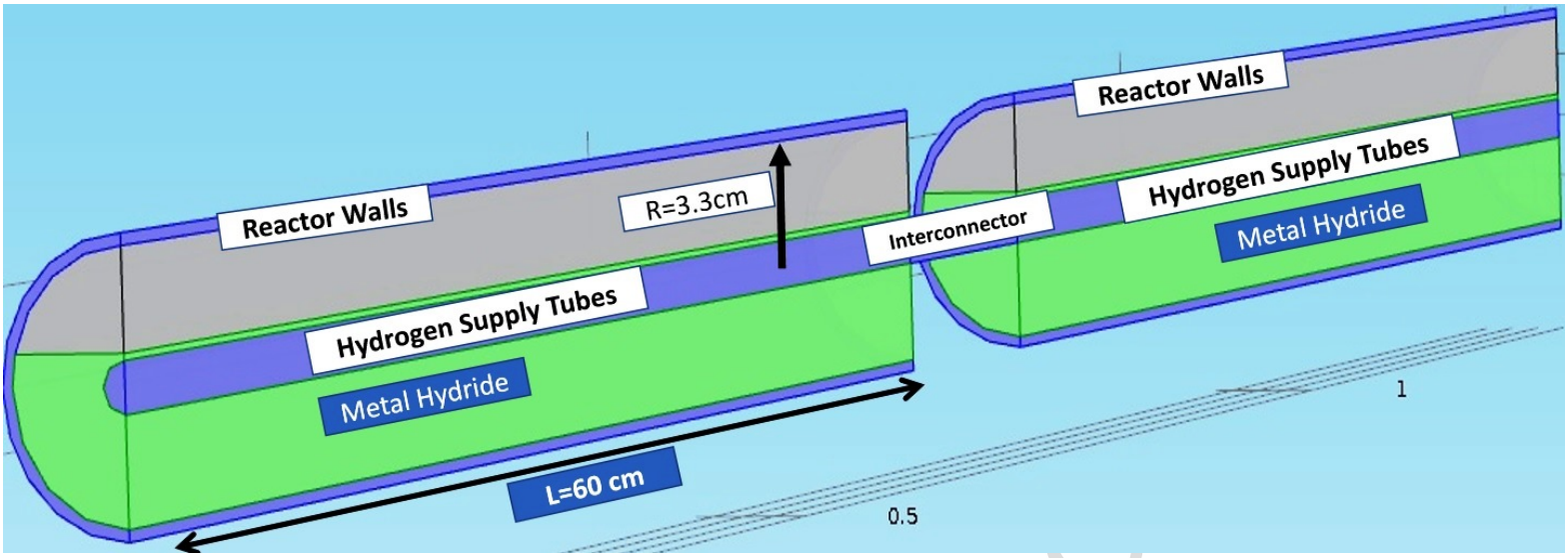

Fig3. The geometry of the reactors used in the current computational study. A cross-section of the reactor (left) shows that the hydride is inside the reactor and the thickness of the walls of the tank chosen to be 3mm. The heating and cooling process is achieved by an external jacket in the current case

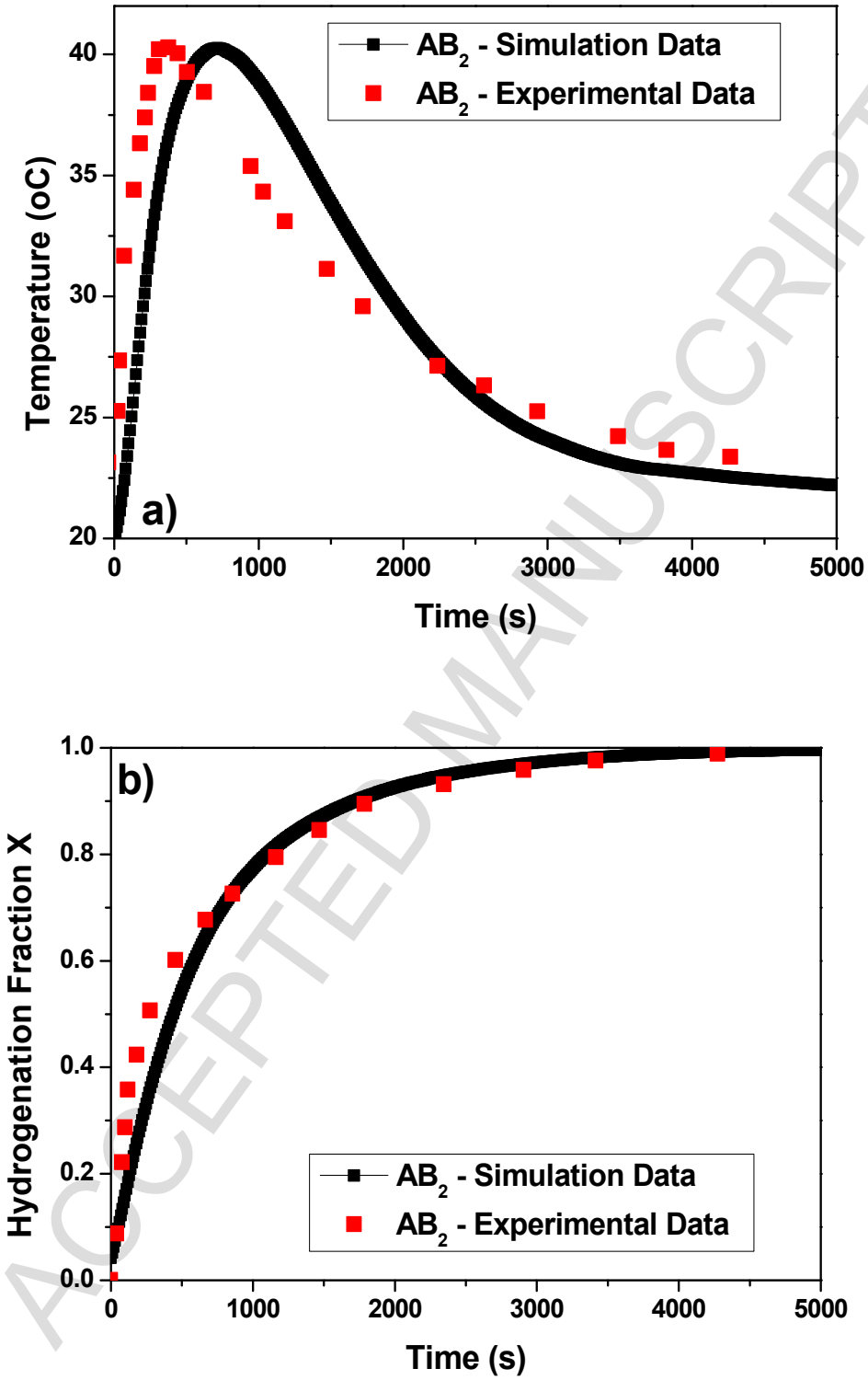

Fig. 4. Validation of the numerical data extracted from the simulation to the experimental results for the synthesized AB_2-Intermetallic. Fig. 4a shows the temperature distribution and Fig. 4b the evolution of the hydrogenation process.

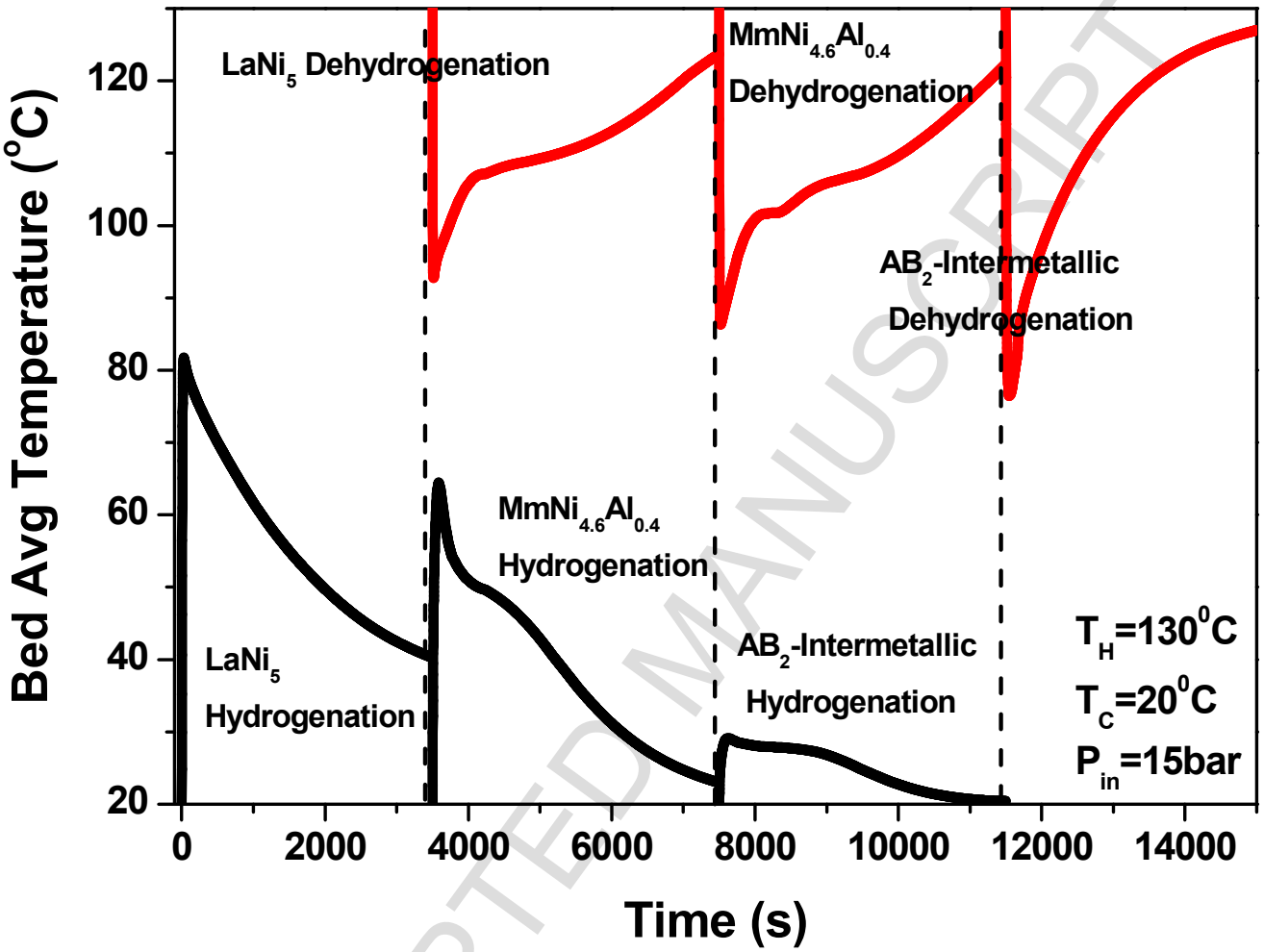

Fig. 5. Bed average temperature evolution during the complete three-stage compression process when using $LaNi_5$, $MmNi_{4.6}Al_{0.4}$ and AB_2-Intermetallic as the stages of the compression.

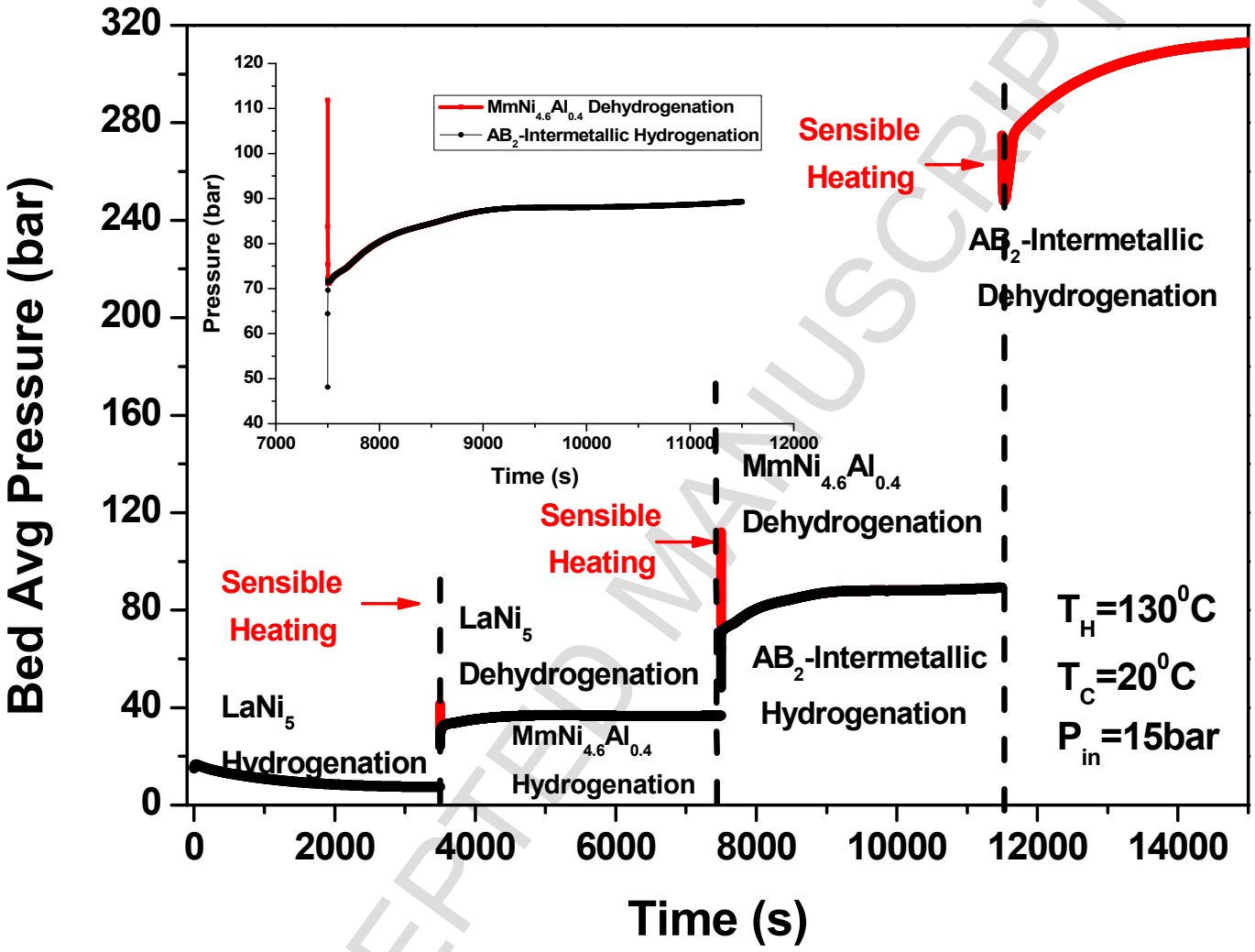

Fig. 6. Bed average pressure evolution during the complete three-stage compression process when using $LaNi_5$, $MmNi_{4.6}Al_{0.4}$ and AB_2-Intermetallic as the stages of the compression.

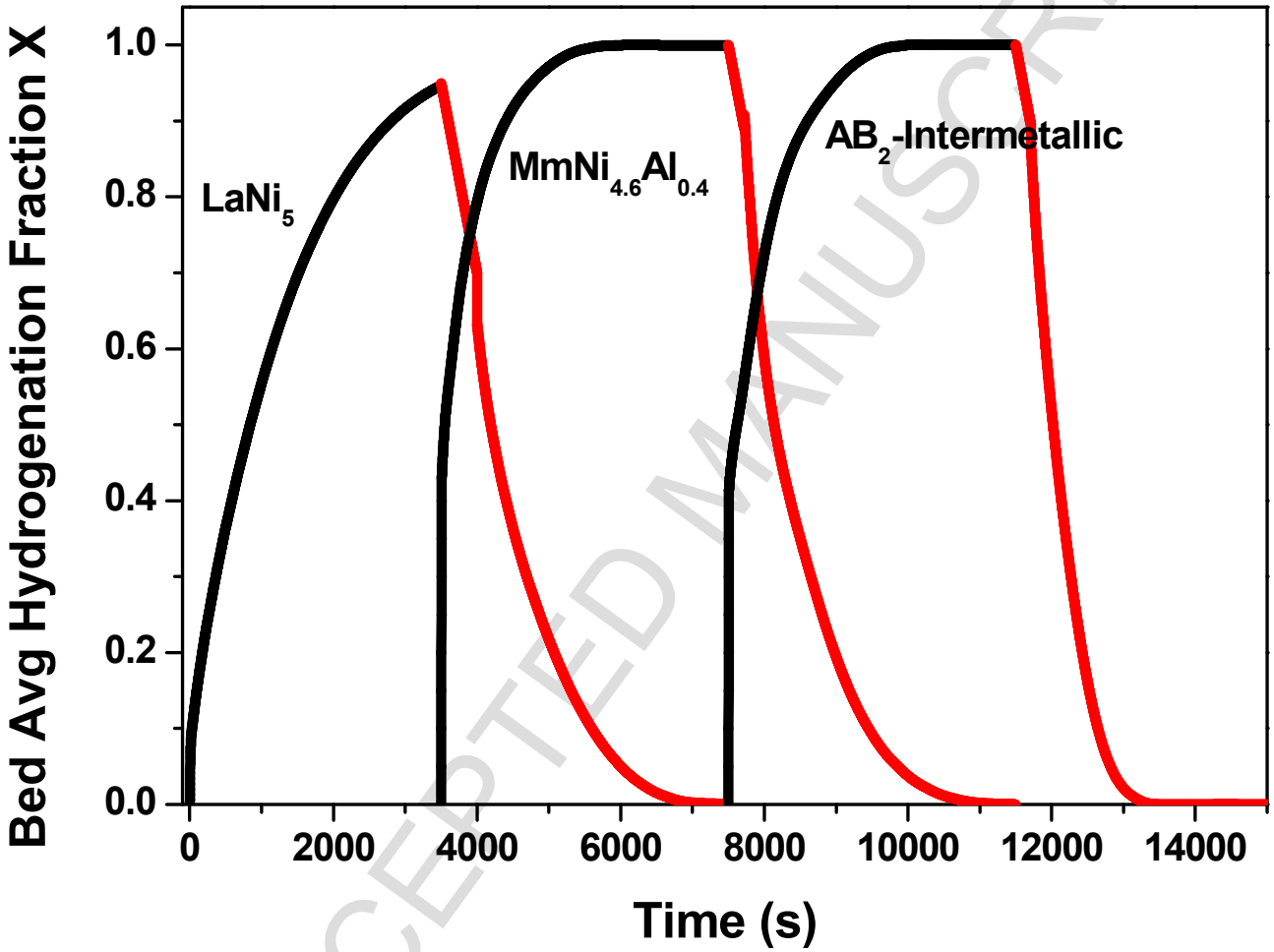

Fig. 7 Bed average hydrogenation/dehydrogenation evolution during the complete three-stage compression process when using $LaNi_5$, $MmNi_{4.6}Al_{0.4}$ and AB_2-Intermetallic as the stages of the compression.

Table 1. Cases used in the current study

	First Stage Alloy	Hydrogenation (20 °C) Dehydrogenation (130 °C)	Second Stage Alloy	Hydrogenation (20 °C) Dehydrogenation (130 °C)	Third Stage Alloy	Hydrogenation (20 °C) Dehydrogenation (130 °C)
Case 1	**$LaNi_5$**	**P_{eq}= 1.94 bar P_{eq}= 41.39 bar**	**$MmNi_{4.6}Al_{0.4}$**	**P_{eq}= 2.69 bar P_{eq}= 111.89 bar**	**Hydralloy C**	**P_{eq}= 31.72 bar P_{eq}= 286.37 bar**
Case 2	**$LaNi_5$**	**P_{eq}= 1.94 bar P_{eq}= 41.39 bar**	**$MmNi_{4.6}Al_{0.4}$**	**P_{eq}= 2.69 bar P_{eq}= 111.89 bar**	**AB_2-Intermetallic**	**P_{eq}= 33.03 bar P_{eq}= 325.75 bar**
Case 3	**$MmNi_{4.6}Al_{0.4}$**	**P_{eq}= 2.69 bar P_{eq}= 111.89 bar**	**Hydralloy C**	**P_{eq}= 31.72 bar P_{eq}= 286.37 bar**	**AB_2-Intermetallic**	**P_{eq}= 33.03 bar P_{eq}= 325.75 bar**

Table 2. Comparison of the operation for the four different MHHC cases

	Cycle Duration (min)	**Compression Ratio**
Case 1	220	19
Case 2	215	22
Case 3	280	23